Nanoscale

PAPER

View Article Online
View Journal | View Issue

Cite this: *Nanoscale*, 2025, **17**, 9245

The role of trap states in MoS_2-based photodetectors†

Yuhang Xu,[a] Yuxin Wang,[a] Chunchi Zhang,[a] Haijuan Wu,[a] Chao Tan,[a] Guohua Hu[b] and Zegao Wang *[a]

Received 26th November 2024,
Accepted 23rd February 2025

DOI: 10.1039/d4nr04974h

rsc.li/nanoscale

Two-dimensional materials show great potential for future optoelectronic device applications, especially in the field of broadband optical detection, due to their high optical responsivity and tunable bandgap structure. In communication and sensing applications, the detection of weak light signals is crucial for improving the quality of signal transmission and the sensitivity of sensors. Although the photogating effect has been shown to provide high light sensitivity, the key features to achieve this dominant light response have not been fully discussed. In this study, we explain in detail the physical mechanism of the photoresponse of molybdenum disulphide-based photodetectors and propose a general basis of judgement for comparing the magnitude of the trap-state action. Through experimental and theoretical analyses, we reveal the physical mechanisms of photocurrents at various stages in the optical ON/OFF switching cycles and provide a theoretical basis for optimising the performance of two-dimensional material-based photodetectors. The results show that the trap states significantly affect the photoresponse characteristics of photodetectors, especially the photocurrent changes at different stages of the optical ON/OFF switching cycles. These findings not only deepen the understanding of the photoelectric properties of two-dimensional materials, but also provide important theoretical guidance for the design of high-performance photodetectors.

Introduction

Converting optical signals into electrical signals is the core of many technologies in our daily life. As a result of advancements in integration methods and high-performance materials, photodetectors are now widely used in security, biomedical imaging, optical communications, motion detection, night vision, and video imaging.[1–3] The existing technology is based on III–V and other optoelectronic traditional semiconductors, including Si, GaN, InGaAs, InSb, and HgCdTe. However, the dark current inherent to these devices necessitates their operation in a low-temperature environment,[4] which is not conducive to the advancement of high-performance, high-integration optoelectronic devices and the development of optoelectronic vision systems.[5–7] In recent years, two-dimensional semiconductors have been shown to have a lower dark current at room temperature due to their two-dimensional structure, where carriers are confined to the planes, resulting in a lower concentration than those of conventional semiconductors.[4,6,7,45,46] However, in contrast to conventional optoelectronic semiconductors, two-dimensional semiconductors tend to have response speeds on the order of milliseconds or even seconds,[8,9] which are not conducive to the construction of high-speed optoelectronic devices.

In recent years, numerous research studies have been conducted with the aim of enhancing their responsivity. These include the use of organic/inorganic surface composites,[10] heterojunction built-in electric field construction,[8,11] and other techniques to modulate the photoelectric excitation and composite paths. This has led to an improvement in photoelectric responsivity. Nevertheless, the mediation has an effect of suppressing responsivity, despite an improvement in the response speed. There is considerable variation in the results obtained by different research groups, particularly in the case of molybdenum disulfide photodetectors. In the two-dimensional (2D) semiconductor photoelectric effect, the prevailing view among researchers is that the photocurrent is influenced by the combined action of photoconductivity, the photothermal effect, and the photovoltaic effect.[12,13] It is commonly accepted that the photocurrent generated in molybdenum disulfide-based photodetectors is a result of the photoconductivity effect and the photogating effect acting in conjunction.[2,4,14,47] However, the precise manner in which these effects influence the performance of two-dimensional semiconductor photodetection and the underlying mechanisms of their respective effects

[a]*College of Materials Science and Engineering, Sichuan University, Chengdu 610065, China. E-mail: zegao@scu.edu.cn*
[b]*Department of Electronic Engineering, The Chinese University of Hong Kong, Shatin, Hong Kong SAR, 999077, China*

† Electronic supplementary information (ESI) available. See DOI: https://doi.org/10.1039/d4nr04974h

remain unclear. Jiang *et al.* pointed that the suppression of deep-trapped energy levels in ReS_2 can significantly reduce the recovery time of the photocurrent.[15] Kufer *et al.* provided a map of the schematic band model of MoS_2 under illumination, but did not offer an analysis of the mechanism of photocurrent generation in the optical ON/OFF switching cycles.[16] However, until now the photoelectric mechanism, especially the role of the interface, is still unclear.

In this study, a molybdenum disulfide-based phototransistor was constructed and the effect of the trap state under gate control and the physical mechanism were investigated. The basis for judging the magnitude of the effect of the trap state action is given by fitting the equation $G \sim P^{\alpha}$ and the competition between the trap energy levels and the composite centers was analysed in detail using a schematic band model. Furthermore, the biexponential relaxation equation was employed to fit the optical ON/OFF switching cycles and the four stages of photocurrents in the optical ON/OFF switching cycle process were extracted. The generation mechanism of photocurrents in each stage was then subjected to detailed analysis. The study in this paper explains the physical mechanism of the photoresponse of molybdenum disulfide-based photodetectors, gives a general judgement basis for comparing the magnitude of the trap-state action, provides a method for the analysis of the physical mechanism of photocurrents at each stage in the optical ON/OFF switching cycles, and provides a theoretical basis for future high-performance photoresponse devices.

Experimental

MoS_2 flakes were micromechanically exfoliated with the standard Scotch-tape method. The flakes were deposited on heavily n-type-doped silicon wafer covered by SiO_2 with a thickness of 285 nm. The source and drain electrodes were fabricated by e-beam lithography followed by e-beam evaporation of 30 nm Ti. For lift-off, the device was soaked in acetone for 10 minutes followed by rinsing with isopropanol. Afterwards, the as-fabricated device was annealed at 523 K for 2 h in Ar gas with a hydrogen concentration of 10% to improve contact conductance. During the measurements, SiO_2 and Si were employed as the insulator layer and back-gate electrode, respectively. All measurements were performed under vacuum conditions using a Keithley 2614B semiconducting device analyzer. The optoelectronic response was measured at a wavelength of 635 nm.

Results and discussion

Fig. 1a and b depict the device schematic and optical image where the channel length L is 5 μm and the thickness of the MoS_2 flakes is about 60 nm. The thickness characterization of MoS_2 is shown in ESI Fig. S1.† Fig. 1c depicts the Raman spectrum of the sample, which was excited at a 532 nm line in an air environment. It can be seen that the vibration modes located at 382 cm^{-1} and 407 cm^{-1} are attributed to the Raman E^1_{2g} and Raman A_{1g} modes.[17,18] In order to eliminate the potential influence of H_2O and O_2 on the device,[19,20] all the electrical tests were conducted in a vacuum probe station. Fig. 1d shows the I_{ds}–V_{ds} curve of sample-1, which exhibits a nonlinear characteristic, indicating a Schottky contact between MoS_2 and the electrodes. The Schottky barrier height generated by the contact of MoS_2 with the electrode can be calcu-

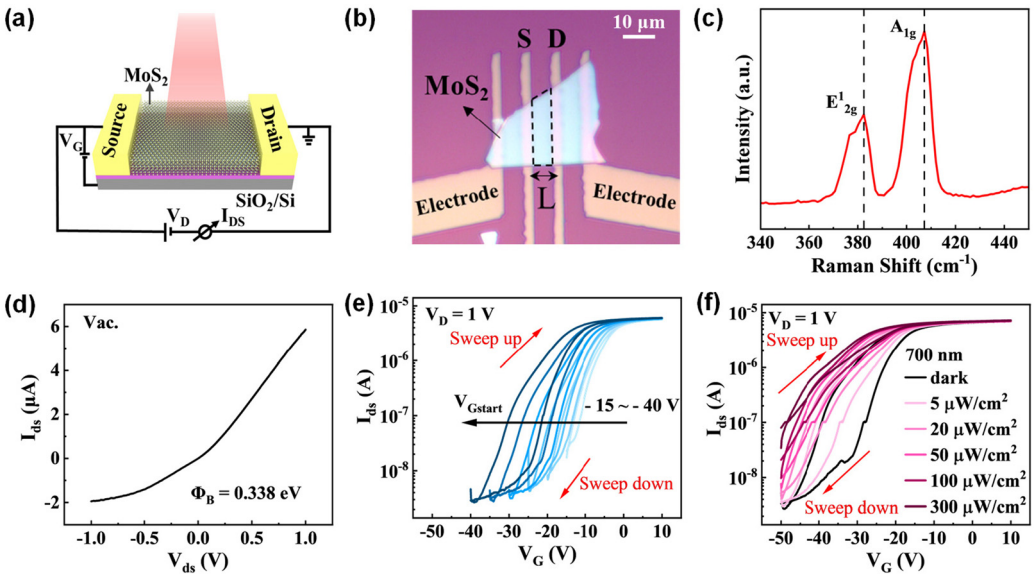

Fig. 1 Device schematic of MoS_2 and its characterization. (a) Schematic and measurement circuit of the device. (b) Optical microscopy image of the MoS_2 phototransistor. (c) Raman characterization of the MoS_2 phototransistor. (d) I_{ds}–V_{ds} characteristics of the MoS_2 phototransistor under dark conditions. (e) Transfer characteristics of the MoS_2 phototransistor in different gate voltage ranges. (f) Transfer characteristics of the MoS_2 phototransistor under illumination with different intensities in bidirectional scanning.

lated from the theory of thermionic electron emission using the following formula:[21]

$$\varnothing = \frac{k_B T}{q}\left(\ln A^* T^2 - \ln\frac{I_0}{S}\right)$$

$$A^* = \frac{4qk_B{}^2 m^*}{h^3}$$

where ∅ represents the Schottky barrier height, k_B is Boltzmann's constant, T is the test temperature, A^* is effective Richardson's constant, I_0 is the reverse saturation current extracted from Fig. 1d, S is the contact area between MoS_2 and the Ti electrodes, m^* is the effective mass of the electrons in MoS_2 ($\sim 0.45m_0$), and h is Planck's constant. It was found that the Schottky barrier height was determined to be 0.338 eV. This is caused by a mismatch in the work function of the material–metal electrode.

The transfer characteristics at varying gate voltage are presented in Fig. 1e. The hysteresis window is defined as the difference between the two voltages when I_{ds} is 10^{-7} A. The hysteresis window of the transfer curves increases with a drop in the starting gate voltage. By fixing the scanning gate voltage range and 700 nm illumination, it can be observed that the hysteresis window (Fig. 1f) decreases with increasing light power, which is in contrast to the results previously reported by Sahoo.[22] Sahoo's findings have demonstrated that the hysteresis window of monolayer MoS_2 increases with increasing optical power. This is the difference between multilayer and monolayer MoS_2.[22] The transfer characteristics at different optical powers at 635 nm are shown in Fig. S3b,† which displayed the same behaviour. Substantial evidence indicates that the hysteresis window is a consequence of sulfur vacancies in intrinsic MoS_2 [23–25] and local states at the MoS_2/SiO_2 interface.[26,27] These defects and local states bring a large number of electron and hole trap levels in the MoS_2 forbidden band gap, where the electron traps are the main cause of the hysteresis window.[22,28]

The density of surface trap states and the concentration of electrons trapped by the electron trapping energy level in the dark and light were calculated from the subthreshold slope,[29,30] as shown in Fig. S2.† In the dark, as the gate voltage drops, the number of surface trap states increases. The electrons are readily captured by the trap level, resulting in a larger hysteresis window. Under illumination, as the power increases, more electrons bound by the trap states are excited to the conduction band to participate in the conductivity, leading to a decrease in the hysteresis window. Conversely, the density of surface trap states increases due to an increase in the number of vacant trap energy levels. In addition, the negative shift of the threshold voltage under light is mainly caused by the photogating effect due to the capture of holes in the trap to form a local state.[27]

As illustrated in Fig. 2, the MoS_2 photodetector exhibits the highest photoresponsivity at 635 nm, which is in accordance with previous reports.[16,31,32] In order to better reveal the physical mechanisms of the devices under light, the role of trap states under illumination was investigated using a 635 nm laser. The transfer characteristics, photoresponsivity *versus* gate voltage and gain *versus* gate voltage for sample-2 are shown in Fig. 2a–c, respectively. The *IV* characteristics of the device are shown in Fig. S3a.† The photoresponsivity was calculated using the following equation: $R = I_{ph}/P_{in}$, where I_{ph} is

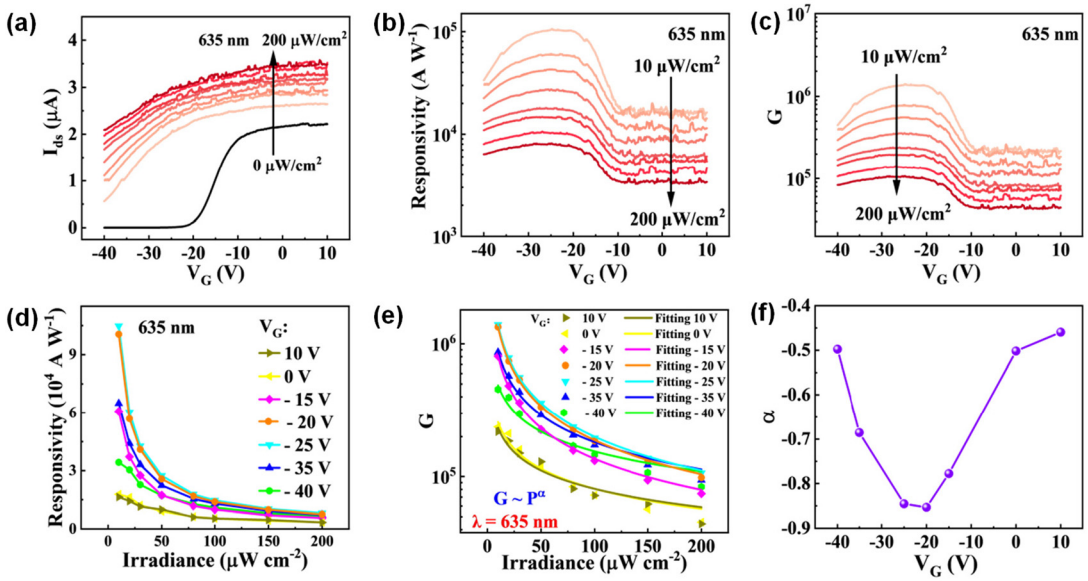

Fig. 2 Optoelectronic response and fitting. (a) Transfer characterization, (b) responsivity and (c) photo gain of the MoS_2 phototransistor under illumination. (d) Optical responsivity and (e) gain of the device *versus* the optical power density at different gate voltages. The solid line in (e) is the fitted curve of gain and optical power. (f) α–V_G curve.

the photocurrent and P_{in} is the incident light power, where the effective illumination area of the device is $S \sim 163\ \mu m^2$. The optical gain is defined as the number of photogenerated electron–hole (e–h) pairs collected by the electrodes to produce the net photocurrent divided by the number of photoexcited e–h pairs. It is given by the following equation: $G = (I_{ph}/e)(PA\eta/h\nu)$. In this paper, the value of η is taken to be 1. Thus, the gain has the same significance as the external quantum efficiency.[22,27] The maximum photoresponsivity R is $\sim 10^5$ A W^{-1} and gain G is $\sim 10^6$ in this certain device. The high photoresponsivity results from a large photo gain. This gain is caused by defects at the SiO_2/MoS_2 interface, defects in MoS_2 itself, and molecules such as H_2O/O_2 absorbed on the material surface.[22,31] The photoresponsivity of MoS_2-based photodetectors in recent research studies is shown in ESI Table S1.† In earlier research,[27] it was found that the process of carrier generation, capture and compounding inside the semiconductor resulted in the exponent $0 < \alpha < 1$ in $I_{ph} \sim P^{\alpha}$. The relationship between responsivity and optical power density was extracted as $R \sim P^{-(1-\alpha)}$. This relationship was also found to be applicable to gain (G). Thus $G \sim P^{\alpha}$ is employed for the fitting process to investigate the underlying physical mechanisms, with the range of α being $-1 < \alpha < 0$. The relationship between $I_{ph} \sim P$ and $G \sim P$ is demonstrated in Fig. S11.† $R \sim P^{\alpha}$ and $G \sim P^{\alpha}$ at different gate voltages are shown in Fig. 2d and e, respectively. With an increase of power, the photoresponsivity decreases, while the change rule of gain and photoresponsivity remains consistent, indicating that optical gain plays a crucial role in the optical response. It is generally accepted that traps result in significant optical gains.[27,33–36] The photoresponsivity is considered to be predominantly influenced by defects. The change of gain with optical power at different gate voltages was fitted with $G \sim P^{\alpha}$, as illustrated by the solid line in Fig. 2e. The parameter α was extracted in order to construct the $\alpha \sim V_G$ curve, as shown in Fig. 2f. When $V_G > -20$ V, α decreases with a decrease in V_G. Conversely, when $V_G < -20$ V, α increases with a decrease in V_G, reaching a minimum value when V_G is approximately -20 V. From the transfer curves, it can be obtained that the threshold voltage V_{th} is ~ -20 V, which coincides with the minimum point of the $\alpha \sim V_G$ curve. As demonstrated in Fig. S10,† the variations in the α values of the remaining devices exhibit a similar trend. The phenomenon that α varies with V_G can be better explained using a schematic band model. Fig. 3a–e show the schematic band model diagrams of the device before and after light illumination at different gate voltages.

When $V_G > V_{th}$, the Fermi level in the dark state is close to the conduction band and the electron traps are almost all filled, while a series of unfilled hole traps lies close to the valence band. Under illumination, several mechanisms contribute to the overall photoresponse as charge carrier excitation, separation, carrier trapping, and recombination. Some of the holes will be captured by the trap states, thereby indirectly participating in the electrical conductivity process and inducing a photocurrent gain.[37] The re-arrangement of electrons and holes under illumination is illustrated in Fig. 3b, which depicts the quasi-electron and hole Fermi levels. The hole initially occupies the deep energy level trap and subsequently the shallow energy level trap. The deep energy level trap exhibits a prolonged lifetime and substantial gain, whereas the shallow energy level trap has a relatively short lifetime and minimal gain.[22,38] This results in a reduction in gain with increasing power density. Further decreasing the V_G, the Fermi level moves away from the conduction band. The hole quasi-Fermi level after illumination moves further closer to the valence band, resulting in more hole deep trap levels being filled and bringing about gain. However, the change of gain is weak at high optical power due to hole shallow trap levels. So as V_G decreases, the change in gain with optical power is more pronounced at low optical power, which leads to a decrease in α.

When $V_G < V_{th}$, the Fermi level is close to the middle band gap, resulting in the exposure of electron traps close to the middle band. These traps act as recombination centers,[16,22] promoting photogenerated carrier complexation and reducing the gain effect. Under illumination, although the hole quasi-Fermi level is closer to the valence band, the presence of the recombination center greatly reduces the carrier lifetime and diminishes the gain effect. At low optical power, the high gain effect of the deep energy level is greatly cut down. At high optical power, some of the photogenerated electrons fill the traps close to the middle band, which reduces the number of recombination centers, so that the gain effect of the shallow trap energy level is not significantly attenuated, which in turn leads to an increase in α. As the V_G decreases, the recombination centers of the intermediate bandgap become increasingly dominant, leading to a further reduction in the gain effect at low optical powers and a continued increase in α. Therefore, α can be used to characterize the effect of trap state gain in the optical response: the smaller the α, the more pronounced the effect of the trap state gain. Fig. S5† shows the gain of sample-3 at different gate voltages: at $V_G < -25$ V, the gain tends to increase and then decrease with optical power. This is caused by the fact that the effect originating from the recombination center at small gate voltage is greater than the trap gain.

In order to further investigate the physical mechanism of the trap state, the device was placed under the same illumination conditions with different gate voltages and the same gate voltage with different illumination conditions for the optical ON/OFF switching cycles test, as shown in Fig. 3e and f, and the light switching time was 5 s. The optical ON/OFF switching cycles of MoS_2-based photodetection at the positive gate voltage are shown in Fig. S4.† Positive gate voltage modulation results in the Fermi energy levels approaching the conduction band and the trap energy levels being filled. This results in a faster speed of response of the device, but with significantly lower I_{on}/I_{off}. To avoid the trap energy level being occupied by holes and no longer functioning after multiple pulses, the first optical ON/OFF switching cycle was selected for the analysis. The optical ON/OFF switching cycles were fitted using a biexponential relaxation

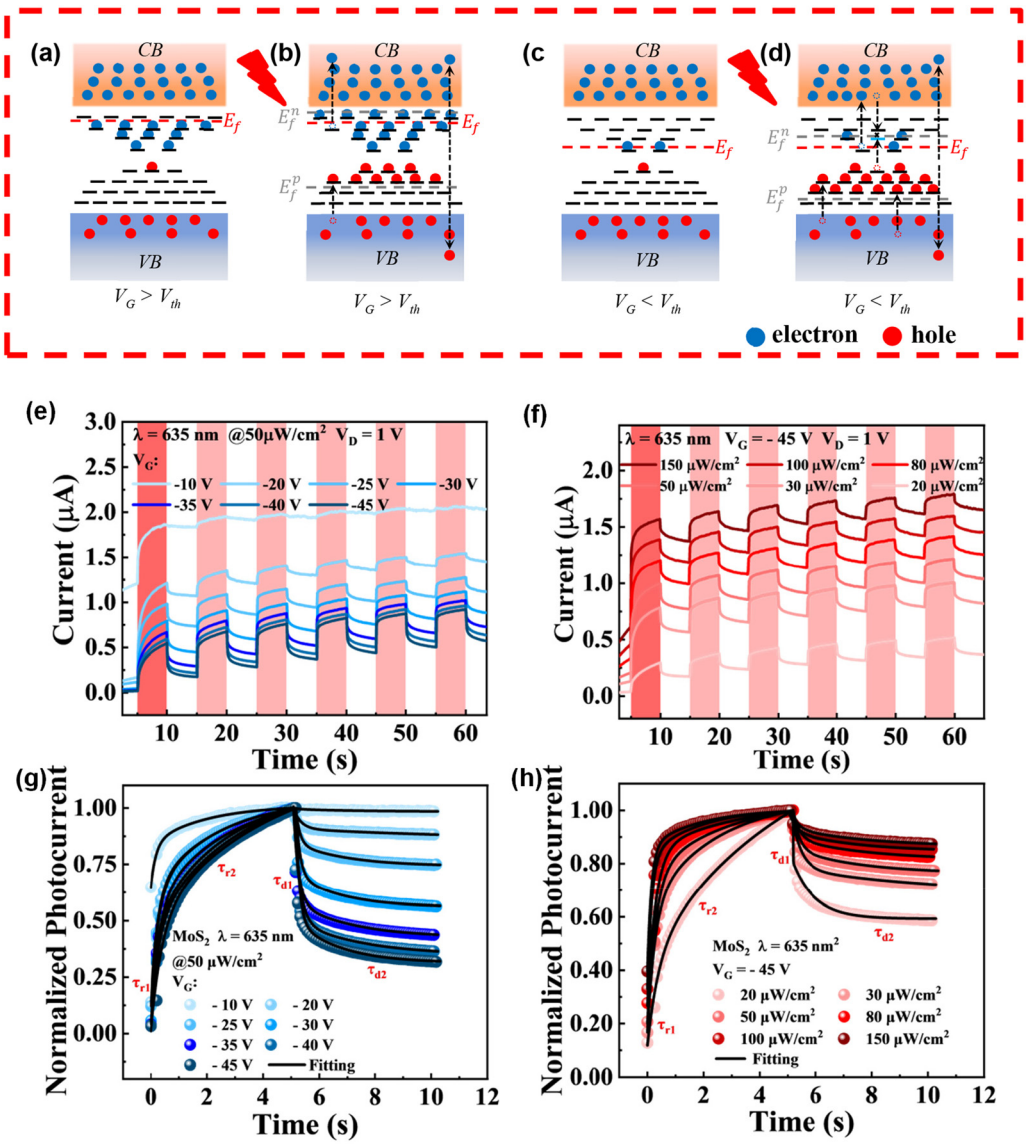

Fig. 3 Mechanism and photoresponsivity. Schematic to explain the behavior of trap states under $V_G > V_{th}$ and $V_G < V_{th}$, respectively. (a) and (b) In the dark and in light at $V_G > V_{th}$, respectively. (c) and (d) In the dark and in light at $V_G < V_{th}$, respectively. (e) Photoresponse of the MoS_2 phototransistor illuminated with 635 nm light with a power of 50 μW cm^{-2} for the optical ON/OFF switching cycles under various gate voltages. (f) Photoresponse of the MoS_2 phototransistor illuminated with different powers of 635 nm light for the optical ON/OFF switching cycles at −45 V gate voltage. The solid lines in (g) and (h) are the fitted curves for the first loop in (e) and (f), respectively.

equation,[39–41] as illustrated in Fig. 3g and h. The corresponding equations are given as follows:[42]

$$I_{ph} = A_1 \exp\left(-\frac{t}{\tau_1}\right) + A_2 \exp\left(-\frac{t}{\tau_2}\right)$$

In the rise edge, the times of the fast process and the slow process are designated as τ_{r1} and τ_{r1}, respectively. The values of the current changes in these two stages were recorded as I_{AB} and I_{BC}, respectively. In the decay edge, the times of the fast process and the slow process are designated as τ_{d1} and τ_{d1}, respectively. The values of the current changes in the two stages were recorded as I_{CD} and I_{DE}, respectively. The extracted four-stage currents are shown in Fig. 4 and the times of the extracted four stages are shown in Fig. S6.†

As illustrated in Fig. 4a, a decrease in α is accompanied by an increase in I_{BC}, while an increase in α is associated with a decrease in I_{BC}. These two variables are strongly correlated. I_{AB} is slightly correlated with α; it is not as strong as the correlation observed for the I_{BC} stage. As demonstrated above, α is a measure of the extent to which trap states contribute to the current. A reduction in α results in an increase in the contribution of trap states to the current, and *vice versa*. This implies that the currents in the AB and BC stage are influenced by trap states. To investigate the mechanism of the trap states in the two stages in detail, the photocurrent was extracted at the

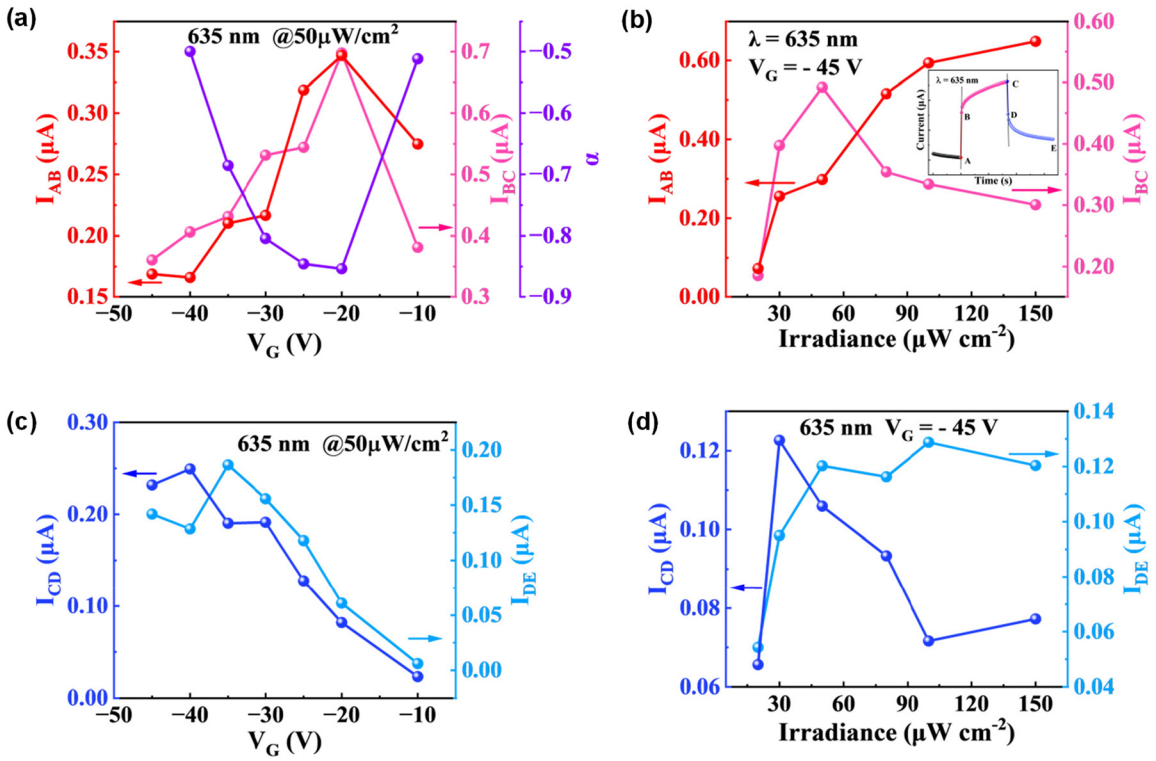

Fig. 4 Photocurrent. (a) Variation of I_{AB}, I_{BC} and α with gate voltage under illumination at 635 nm at a power of 50 μW cm^{-2}. (b) Variation of I_{AB} and I_{BC} with optical power at a gate voltage of −45 V. The inset shows the segmentation of the optical ON/OFF switching curve. (c) Variation of I_{CD}, I_{DE} and α with gate voltage under illumination at 635 nm at a power of 50 μW cm^{-2}. (d) Variation of I_{AB} and I_{BC} with optical power at a gate voltage of −45 V.

same gate voltage, as illustrated in Fig. 4b. I_{AB} increases with increasing optical power; the higher the optical power, the more electron–hole pairs are excited, and the larger the response photocurrent. However, I_{AB} exhibits a slight nonlinearity with respect to the optical power density, which can be attributed to the trap state.[8,14] Additionally, the response speed of the AB stage is rapid, suggesting that this stage is predominantly influenced by the gain caused by shallow traps, as well as photoconductivity effects. On the other hand, I_{BC} increases first and then decreases with optical power. This is due to the fact that at low optical power, deep traps exert a dominant influence, whereas at high optical power, shallow traps play a dominant role. Consequently, with an increase of optical power density, the I_{BC} trend initially rises and subsequently declines.[16]

The photocurrent in the CD and DE stages is mainly related to the role of the recombination centers; as the gate voltage drops at the same optical power, the number of recombination centers increases, causing the current of the two decline stages to increase simultaneously, as shown in Fig. 4c. The reason for the reduction of photocurrent in the two stages is further distinguished by extracting the photocurrent at the same gate voltage, as shown in Fig. 4d. For the CD stage, because both I_{AB} and I_{BC} are small, the falling current $|I_{CD}|$ is minimal at low power. As the optical power increases, the photocurrent becomes larger, resulting in more free carriers being rapidly trapped by the recombination centers and the falling photocurrent $|I_{CD}|$ increases rapidly. When the optical power continues to increase, part of the recombination centers is filled with electrons, resulting in a decrease in the falling photocurrent $|I_{CD}|$. Therefore, at $V_G < V_{th}$, $|I_{CD}|$ shows a trend of first increasing and then decreasing. When the recombination centers are completely filled, the carriers trapped in the shallow trap energy level do not recombine immediately. The lifetime of the carriers at the shallow trap energy level is longer than photoexcited electron–hole pairs and at this time, the current in the CD stage is mainly dominated by the photoconductivity effect. Therefore, after illuminating with 100 μm cm^{-2}, the number of electron–hole pairs generated by direct photoexcitation increases and participates in the conductivity, which leads to an inflection point.

The direct recombination of photogenerated carriers as well as the recombination center-assisted recombination makes the recombination fast.[43] Due to the existence of the trap level, the decay time of the DE stage is longer. At low optical power, $|I_{DE}|$ is small due to the small photocurrent. As the optical power increases, the current induced by trap states increases. At a certain optical power, the trap level was completely filled, resulting in the current gain no longer increasing. Therefore $|I_{DE}|$ shows a trend of increasing and then stabilising with increasing optical power. The speed of response *versus* gate voltage is shown in Fig. S7.† Fig. S8 and S9† illustrate the

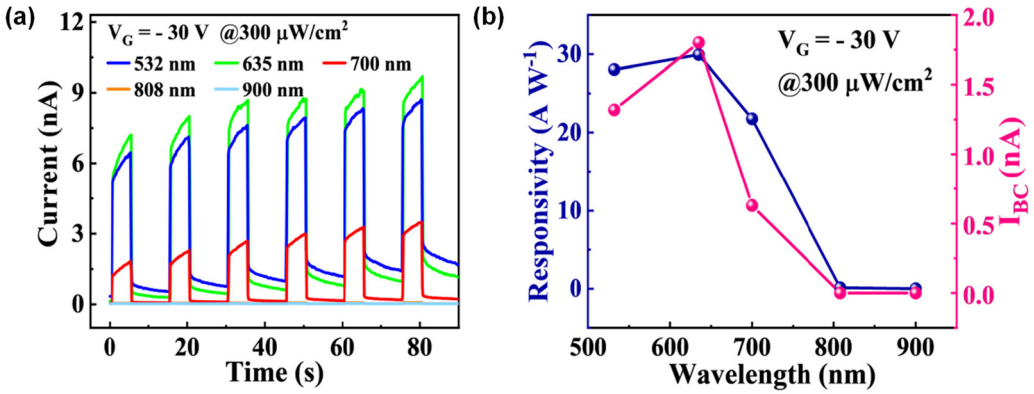

Fig. 5 Phototransistor metrics. (a) Photocurrent of the MoS_2 phototransistor at different wavelengths. (b) Response and I_{BC} with wavelength at a gate voltage of −30 V and an optical power of 300 μW cm^{-2}.

pattern of change between the current and the source–drain voltage for the four stages of sample-4 at different gate voltages, where $|I_{DE}|$ at V_G = −35 V shows a decreasing trend with increasing source–drain voltage. The presence of a considerable number of recombination centers at relatively low gate voltages may be a contributing factor. As the source–drain voltage increases, the kinetic energy of the free carriers increases, leading to greater motion and higher probability of electron complexes. This leads to a significant number of free carriers being recombined in the CD section, while the current change in the DE section is reduced.

With all other conditions being the same, different wavelengths of laser light were used to irradiate sample-3 and the corresponding optical ON/OFF switching are shown in Fig. 5a. The photocurrents in the BC stage under the first pulse of the optical ON/OFF switching curve at different wavelengths were extracted and their variations were consistent with the photoresponsivity. This phenomenon results from the generation of more photogenerated carriers trapped by trap states in the sensitive wavelength of MoS_2. This leads to a positive correlation between the I_{BC} and the sensitivity of the material to the wavelength. It should be noted that since the physical properties of MoS_2 are independent of thickness when it exceeds 5 layers,[44,48] we did not investigate the thickness effect in this study.

Conclusions

In summary, multilayer MoS_2 photodetectors with a channel length of 5 μm were prepared. The hysteresis window of transfer increases with decreasing gate voltage and decreases with increasing optical power due to the increase of the electronic surface trap states of the device with the drop of gate voltage and the excitation of the electrons in the trap states to the conduction band to participate in the conductivity under light. The high responsivity of the device, which has a value of approximately $R \sim 10^5$ A W^{-1}, can be attributed to the high gain, which has a value of approximately $G \sim 10^6$, resulting from the material's trap state. By fitting $G \sim P^{\alpha}$ and extracting α at different gate voltages and analysing it in combination with a schematic band model, it can be concluded that α is a suitable parameter for characterizing the effect of the trap state gain in the optical response. Furthermore, it can be demonstrated that the gate voltage corresponding to the maximum gain effect is the threshold voltage V_{th}. The optical ON/OFF switching curves for a given optical power with different gate voltages and for the same gate voltage with different optical powers were fitted using a biexponential relaxation equation. Furthermore, the physical mechanisms of the dominant photocurrents in the different stages were analysed by extracting the current variations in the four stages. The above analysis method can also be used for the analysis of other two-dimensional semiconductor optoelectronic devices, which provides a methodological basis for the surface engineering and defect engineering of two-dimensional optoelectronic materials. Concurrently, this approach provides a theoretical foundation for the advancement of two-dimensional semiconductor photodetectors with enhanced responsivity and rapid response times.

Author contributions

Z.W. conceived, designed and supervised the project. Y.X., Y. W., C.Z. and H.W. conducted the experimental work. Y.X., C.T. and G.H. performed the data analysis. Y.X. and Z.W. wrote the manuscript. All authors contributed to the discussion of the results and editing of the manuscript.

Data availability

The data supporting this article have been included as part of the ESI.†

Conflicts of interest

There are no conflicts to declare.

Acknowledgements

This work was financially supported by the National Natural Science Foundation of China (52272160, U2330112 and 52002254) and the Sichuan Science and Technology Foundation (2025YFHZ0102 and 2024JDRC0021).

References

1 F. H. L. Koppens, T. Mueller, P. Avouris, A. C. Ferrari, M. S. Vitiello, *et al.*, *Nat. Nanotechnol.*, 2014, **9**, 780–793.
2 G. Mu, Y. M. Tan, C. Bi, Y. F. Liu, Q. Hao, *et al.*, *Nat. Photonics*, 2024, **18**, 1147–1154.
3 J. X. Liu, Z. H. Peng, C. Tan, L. Yang, R. D. Xu, *et al.*, *Front. Phys.*, 2024, **19**, 62502.
4 M. S. Long, P. Wang, H. H. Fang and W. D. Hu, *Adv. Funct. Mater.*, 2019, **29**, 1803807.
5 R. J. Tian, X. T. Gan, C. Li, X. Q. Chen, S. Q. Hu, *et al.*, *Light: Sci. Appl.*, 2022, **11**, 101.
6 X. L. Zhang, R. Z. Li, Y. F. Yu, F. X. Dai, R. Q. Jiang, *et al.*, *Laser Photonics Rev.*, 2024, **18**, 2300936.
7 P. Jin, Y. J. Tang, D. W. Li, Y. Wang, P. Ran, *et al.*, *Nat. Commun.*, 2023, **14**, 626.
8 M. Liu, J. Wei, L. Qi, J. An, X. Liu, *et al.*, *Nat. Commun.*, 2024, **15**, 141.
9 Z. Liu, X. Y. Jia, W. S. Duan, X. F. Zhu, B. He, *et al.*, *Adv. Opt. Mater.*, 2023, **11**, 2202087.
10 C. Li, H. Wang, F. Wang, T. Li, M. Xu, *et al.*, *Light: Sci. Appl.*, 2020, **9**, 31.
11 N. Flöry, P. Ma, Y. Salamin, A. Emboras, T. Taniguchi, *et al.*, *Nat. Nanotechnol.*, 2020, **15**, 118.
12 C. Y. Liu, J. S. Guo, L. W. Yu, J. Li, M. Zhang, *et al.*, *Light: Sci. Appl.*, 2021, **10**, 123.
13 Q. X. Qiu and Z. M. Huang, *Adv. Mater.*, 2021, **33**, 2008126.
14 R. Nur, T. Tsuchiya, K. Toprasertpong, K. Terabe, S. Takagi, *et al.*, *Commun. Mater.*, 2020, **1**, 103.
15 J. Jiang, C. Y. Ling, T. Xu, W. H. Wang, X. H. Niu, *et al.*, *Adv. Mater.*, 2018, **30**, 1804332.
16 D. Kufer and G. Konstantatos, *Nano Lett.*, 2015, **15**, 7307–7313.
17 P. A. Bertrand, *Phys. Rev. B:Condens. Matter Mater. Phys.*, 1991, **44**, 5745–5749.
18 H. Li, Q. Zhang, C. C. R. Yap, B. K. Tay, T. H. T. Edwin, *et al.*, *Adv. Funct. Mater.*, 2012, **22**, 1385–1390.
19 Y. W. Zhang, H. Li, L. Wang, H. M. Wang, X. M. Xie, *et al.*, *Sci. Rep.*, 2015, **5**, 7938.
20 P. Han, E. R. Adler, Y. J. Liu, L. St Marie, A. El Fatimy, *et al.*, *Nanotechnology*, 2019, **30**, 284004.
21 N. Kaushik, A. Nipane, F. Basheer, S. Dubey, S. Grover, *et al.*, *Appl. Phys. Lett.*, 2014, **105**, 113505.
22 S. Sahoo, M. C. Sahu, S. K. Mallik, A. K. Jena, G. K. Pradhan and S. Sahoo, *ACS Appl. Electron. Mater.*, 2023, **5**, 1077–1087.
23 S. Fu, J. H. Park, H. Gao, T. Y. Zhang, X. Ji, *et al.*, *Nano Lett.*, 2023, **23**, 5869–5876.
24 F. Li, R. Tao, B. L. Cao, L. Yang and Z. G. Wang, *Adv. Funct. Mater.*, 2021, **31**, 2104367.
25 X. Y. Xiong, F. Wu, Y. Ouyang, Y. M. Liu, Z. G. Wang, *et al.*, *Adv. Funct. Mater.*, 2024, **34**, 2213348.
26 X. T. Guo, W. H. Wang, H. Y. Nan, Y. F. Yu, J. Jiang, *et al.*, *Optica*, 2016, **3**, 1066–1070.
27 H. H. Fang and W. D. Hu, *Adv. Sci.*, 2017, **4**, 1700323.
28 Z. H. Peng, X. I. Luo, K. X. Liang, C. Tan, L. B. Gao and Z. G. Wang, *Adv. Opt. Mater.*, 2023, **11**, 2202378.
29 A. Sebastian, R. Pendurthi, T. H. Choudhury, J. M. Redwing and S. Das, *Nat. Commun.*, 2021, **12**, 693.
30 B. L. Cao, Z. G. Wang, X. Y. Xiong, L. B. Gao, J. H. Li, *et al.*, *New J. Chem.*, 2021, **45**, 12033–12040.
31 C. L. Wang, Q. Q. Wu, Y. Ding, X. M. Zhang, W. H. Wang, *et al.*, *ACS Appl. Mater. Interfaces*, 2023, **15**, 46236–46246.
32 X. Y. Liu, J. Q. Zhu, Y. F. Shan, C. L. Liu, C. Y. Pan, *et al.*, *Adv. Sci.*, 2024, **11**, 2408299.
33 Q. H. Zhao, W. Wang, F. Carrascoso-Plana, W. Q. Jie, T. Wang, *et al.*, *Mater. Horiz.*, 2020, **7**, 252–262.
34 H. Jiang, J. T. Fu, J. X. Wei, S. J. Li, C. B. Nie, *et al.*, *Nat. Commun.*, 2024, **15**, 1225.
35 Q. J. Liang, Q. X. Wang, Q. Zhang, J. X. Wei, S. X. D. Lim, *et al.*, *Adv. Mater.*, 2019, **31**, 1807609.
36 L. Li, W. K. Wang, Y. Chai, H. Q. Li, M. L. Tian, *et al.*, *Adv. Funct. Mater.*, 2017, **27**, 1701011.
37 G. Konstantatos, M. Badioli, L. Gaudreau, J. Osmond, M. Bernechea, *et al.*, *Nat. Nanotechnol.*, 2012, **7**, 363–368.
38 S. G. Seo, J. Joeng, K. Kim, K. Kim and S. H. Jin, *IEEE Trans. Electron Devices*, 2020, **67**, 1864–1872.
39 H. L. Wang, X. D. Wang, Y. Chen, S. K. Zhang, W. Jiang, *et al.*, *Adv. Opt. Mater.*, 2020, **8**, 1901402.
40 A. George, M. V. Fistul, M. Gruenewald, D. Kaiser, T. Lehnert, *et al.*, *npj 2D Mater. Appl.*, 2021, **5**, 15.
41 M. M. Islam, D. Dev, A. Krishnaprasad, L. Tetard and T. Roy, *Sci. Rep.*, 2020, **10**, 21870.
42 Q. H. Ren, W. H. Xu, Z. H. Shen, T. G. You, Q. Liu, *et al.*, *ACS Appl. Electron. Mater.*, 2021, **3**, 451–460.
43 M. Y. Wang, X. X. Zheng, X. L. Ye, W. C. Liu, B. Q. Zhang, *et al.*, *Nano Lett.*, 2023, **24**, 165–171.
44 M. W. Lin, I. I. Kravchenko, J. Fowlkes, X. F. Li, A. A. Puretzky, C. M. Rouleau, *et al.*, *Nanotechnology*, 2016, **27**, 165203.
45 J. X. Liu, C. C. Zhang, Y. Huang, H. J. Wu, C. Tan, *et al.*, *Nanoscale*, 2024, **16**, 22403–22410.
46 X. Du, H. J. Wu, Z. H. Peng, C. Tan, L. Yang, *et al.*, *Mater. Sci. Eng., R*, 2024, **161**, 100839.
47 C. Tan, Z. H. Yang, H. J. Wu, Y. Yang, L. Yang and Z. G. Wang, *Nanoscale*, 2024, **16**, 6241–6248.
48 Z. G. Wang, Q. Li, Y. F. Chen, B. X. Cui, Y. R. Li, F. Besenbacher, *et al.*, *NPG Asia Mater.*, 2018, **10**, 703–712.

